Journal of Materials Chemistry A

Accepted Manuscript

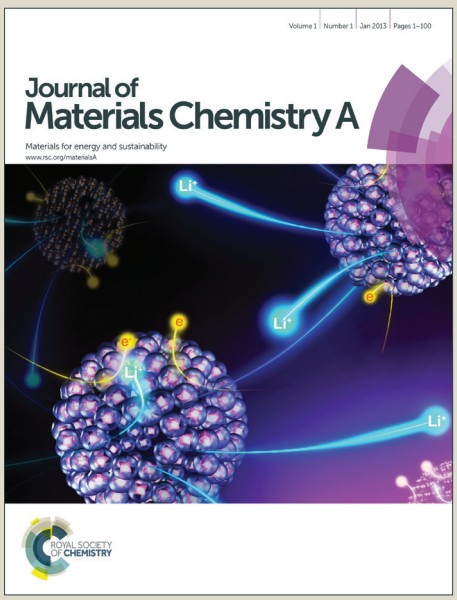

ROYAL SOCIETY OF CHEMISTRY

www.rsc.org/materialsA

Ni@NiO Core-Shell Nanoparticle Tube Arrays with Enhanced Supercapacitor Performance

Qi Li,[†] Chao-Lun Liang,[†,‡] Xue-Feng Lu,[†] Ye-Xiang Tong,*[,†] and Gao-Ren Li*[,†]

[†]*MOE Laboratory of Bioinorganic and Synthetic Chemistry, KLGHEI of Environment and Energy Chemistry, School of Chemistry and Chemical Engineering, Sun Yat-sen University, Guangzhou 510275, China*

[‡]*Instrumental Analysis and Research Centre, Sun Yat-Sen University, Guangzhou 510275, China*

E-mail: ligaoren@mail.sysu.edu.cn

ABSTRACT

Nanotube arrays have shown great potentials in a variety of important applications, such as energy storage. To enhance the inherent properties and endow nanotubes with multifunctionality, the rational design of nanotube arrays with higher complexity in terms of structure and composition are highly desired and still remains a great challenge. In this work, the Ni@NiO core-shell nanoparticle tube arrays (CSNPTAs) were designed and fabricated via an efficient, low-cost and environmental friendly ZnO nanorods template-assisted electrodeposition method, and they are effective in enhancing ion diffusion and surface area as well as preventing nanoparticle agglomeration because of the unique array structures, hollow structures, and core-shell nanoparticle structures. As electrodes, the Ni@NiO CSNPTAs show high electrochemical performance such as high specific capacitance (C_{sp}), superior rate capability, and excellent cycle stability and exhibit promising applications for high-performance supercapacitors (SCs).

1. Introduction

Nanotubes with hollow and anisotropic structures have recently been the focus of tremendous interest because of their great potential in various applications, including energy conversion and storage, catalysis, drug delivery, and gas sensors.[1-4] In the past decade, there has been great success in developing the effective synthesis methods for the fabrication of nanotubes.[5-7] However, most of the structures of nanotubes reported in literatures are relatively simple.[8-11] Recently, researchers worldwide have concentrated rapidly increasing efforts on the rational design and synthesis of complex nanotubes.[12-15] The nanotube structures with higher complexity in terms of structure and composition are expected to offer exciting opportunities for both fundamental studies and practical applications.[16]

Recently, the nanoparticle tubes (NPTs) have attracted great interest because the combination of nanotube geometry with nanoparticle morphology will achieve the hollow structure, anisotropic structure, high surface-to-volume ratio, small size effect and synergistic effect,[17-21] which all are highly appealing in the design and synthesis of electrochemical energy materials. However, up to now, the complex NPTs, such as core-shell nanoparticle tube arrays (CSNPTAs), were rarely reported.[22] With increasing demand for advanced func-tional materials, the core-shell nanoparticles, representing multiple-discrete functions related components integrated in one unit, have recently been subjected to extensive research because of their promisingly wide applications in the renewable energy, advanced bio-medicine, and environmental cleanup due to the rich heterogeneous interfaces and synergistic effects between the different components.[23-25] Thus, based on the unique core-shell nanoparticles, the novel CSNPTAs will attract great interest because they are effective in enhancing ion diffusion and surface area as well as preventing nanoparticle agglomeration.

Here the Ni@NiO CSNPTAs were designed and fabricated via a low-cost and environmental-friendly ZnO nanorod template-assisted electrodeposition that has been proved to be a simple and efficient method for the design and synthesis of nanotubes.[26-27] NiO has been considered to be one of the most attractive electrode materials for supercapacitors because of its low cost, high abundance, high theoretical specific capacitance (C_{sp}), and environmental friendliness.[28-32] The Ni@NiO CSNPTAs can efficiently improve the

transmission of electroactive species because of the porous structures, core-shell structures, nanotube structures and high order arrays, and they show promising utilization in the energy storage systems.[31-35] Hence, it is expected that more diverse functional properties can be introduced into NiO by designing Ni@NiO CSNPTAs. In this study, we present the rational design and fabrication of Ni@NiO CSNPTAs and the promising applications for high-performance supercapacitors (SCs).

2. Results and Discussion

The schematic illustration of the procedures used to fabricate Ni@NiO CSNPTAs is shown in Scheme 1. After the fabrication of ZnO nanorod arrays (NRAs), Ni nanoparticle layers were electrodeposited on the surfaces of ZnO NRAs to form ZnO@Ni NRAs. Ni nanoparticle tube arrays (NPTAs) were then fabricated by dissolving ZnO templates from the ZnO@Ni NRAs in 3% $NH_3 \cdot H_2O$ solution. Finally, the Ni@NiO CSNPTAs were successfully fabricated via the partial oxidation of Ni NPTAs by heat treatment in air. The details of the fabrication procedures of Ni@NiO CSNPTAs are described in the experimental section. SEM images of ZnO NRAs are shown in Figure 1a-b, which shows hexagonal ZnO nanorods were fabricated. The diameters of ZnO nanorods are 300~400 nm, and the lengths are ~2.0 μm. SEM images of the ZnO@Ni NRAs are shown in Figure 1c-d, which shows ZnO nanorods have uniform Ni nanoparticle wraps. After dissolving ZnO, the Ni NPTAs were fabricated and their SEM images with different magnifications are shown in Figure 1e-f, which shows Ni NPTAs have porous structures and are composed of nanoparticles. SEM image of a broken Ni nanotube is shown in inset in Figure 1f, which shows hollow nanotube structure. TEM image of a typical Ni nanotube is shown in Figure 1g, which further proves the hollow tube structures are composed of nanoparticles. The diameters of Ni nanotubes are 500~600 nm and wall thicknesses are ~100 nm. The lengths of Ni nanotubes are ~2.0 μm. The results of HRTEM and SAED in Figure 1h show that the Ni nanotubes are polycrystalline. XPS spectra of the Ni NPTAs are shown in Figure 1*i*. The strong peaks located at 852.7 and 869.9 eV correspond to metal Ni,[36] and almost no NiO peak is seen. The XPS results prove Ni NPTAs were obtained.

To fabricate Ni@NiO CSNPTAs, here we performed the partial oxidation of Ni NPTAs. The oxidation

of Ni NPTAs was studied by thermogravimetric (TG) analysis under an atmosphere of air and the TG profile is shown in Figure 2a. With temperature increasing, approximately 22% weight increment was seen up to 500 °C, and this was attributed to the oxidation of Ni NPTAs. Above 500 °C, the weight change of the sample was almost stable, suggesting that the oxidation of Ni NPTAs was almost completion. Based on the result of TG, we carried out the partial oxidation of Ni NPTAs at 350 ^{0}C for 60 min. Before heat treatment, XRD pattern of the Ni NPTAs is shown in Figure 2b, which proves the existence of metal Ni in the sample. After heat treatment at 350 ^{0}C for 60 min, XRD pattern of the sample is shown in Figure 2c, which proves the coexistence of Ni and NiO in the sample, indicating the partial oxidation of Ni NPTAs. After heat treatment at 350 ^{0}C for 180 min, Ni NPTAs were completely oxidized to form NiO NTAs as shown in Figure 2d, which only shows NiO peaks. Here we carried out the oxidation of Ni NPTAs at 350 ^{0}C for 60 min to fabricate Ni@ NiO CSNPTAs.

SEM images of Ni@NiO CSNPTAs with different magnifications are shown in Figure 3a-b, which show Ni@NiO CSNPTAs have porous structures and are composed of nanoparticles. TEM images of Ni@NiO CSNPTAs with different magnifications are shown in Figure 3c-d, which further show porous and hollow nanotube structures and they are composed of nanoparticles. The diameters of Ni@NiO CSNPTAs are 500~600 nm and wall thicknesses are ~100 nm. The lengths of NiO CSNPTAs are ~2.0 μm. The sizes of nanoparticles are 50~100 nm. The magnified TEM image and the HRTEM image of a typical nanoparticle in Ni@NiO CSNPTAs is shown in Figure 3e and 3f, respectively, which both clearly prove the core-shell structure. The SAED pattern shown in Figure 3f shows that the Ni@NiO nanoparticle is polycrystalline (inset in Figure 3f). The distributions of elements Ni and O in the Ni@NiO CSNPTAs were studied by STEM/EDX analysis. STEM image of Ni@NiO nanoparticles is shown in Figure 3g. The corresponding EDX map of element Ni is shown in Figure 3h, which shows that the Ni is uniformly dispersive. However, the distribution of element O in the same area is not uniformly as shown in Figure 3*i*, and the black holes exist in the EDX map of O as marked with white rings. Compared with EDS map of Ni in Figure 3h, the black holes in the EDX map of O in Figure 3i indicate the existence of Ni cores in these nanoparticles. Therefore, based on the above results of TEM and EDS maps, the Ni@NiO CSNPTAs were successfully

fabricated.

X-ray photoelectron spectroscopy (XPS) analysis of Ni@NiO CSNPTAs was carried out, and XPS profiles of Ni 2p and O 1s regions are presented in Figure 3*j* and 3*k*, respectively. The Ni 2p spectrum can be deconvoluted into five peaks as shown in Figure 3*j*. The peaks located at 852.2 and 869.4 eV (red line) correspond to Ni^0 state, and the peaks located at 856.1, 861.5 and 873.6 eV (blue line) correspond to Ni^{2+} state,[30] indicating the coexistence of Ni^0 and Ni^{2+} in Ni@NiO CSNPTAs. According to O 1s spectrum in Figure 3*k*, one peak at 531.9 eV is seen and it can be assigned to O^{2-} in NiO. Therefore, the above XPS results also demonstrate the coexistence of Ni and NiO in Ni@NiO CSNPTAs.

Compared with NiO nanotube arrays (NTAs), the fabricated Ni@NiO CSNPTAs can obviously improve the electron transfer and collection because of the high conductivity of metal Ni. The Nyquist plot of the Ni@NiO CSNPTAs between 1 Hz and 10 kHz is shown in Figure 3L, which shows Ni@NiO CSNPTAs have smaller charge transfer resistance than NiO NTAs, thus improving the transport and collection of electrons in electrode. The higher conductibility of Ni@NiO CSNPTAs than NiO NTAs will favour rate capability for high power performance and fast charge/discharge. The utilization rate of electrodes will also be largely enhanced by the high conductibility because of slight polarization.

By combining the metal@metal oxide core-shell nanoparticles and nanotube arrays, the electrochemical performance of Ni@NiO CSNPTAs can be markedly enhanced. Cyclic voltammograms (CVs) of the Ni@NiO CSNPTAs and NiO NTAs at 50 mV/s in a half-cell (three electrode configuration) are shown in Figure 4a, which shows two pairs of redox peaks, indicating good redox transitions of NiO between the different valence states. In addition, the high symmetrical CV characteristics in forward and reverse scans are seen. These results show a good pseudocapacitive response of NiO arising from reversible Faradaic reactions on the electrode surface. Compared with NiO NTAs, the Ni@NiO CSNPTAs show larger CV area as shown in Figure 4a, indicating the specific capacitance (C_{sp}) of Ni@NiO CSNPTAs is significantly enhanced after constructing core-shell structures. The Ni@NiO CSNPTAs achieve a large C_{sp} of 949 F g^{-1} at a scan rate of 5 mV s^{-1} for whole electrode, and at a high scan rate of 50 mV s^{-1} they still achieve a large C_{sp} of 713 F g^{-1}, which is much larger than 417 F/g of NiO NTAs at the same scan rate. CVs of the

Ni@NiO CSNPTAs at various scan rates are shown in Figure 4b, and the dependence of C_{sp} on scan rate is shown in Figure 4c. Ni@NiO CSNPTAs show excellent rate capability and C_{sp} decay from 5 to 100 mV/s is only ~33%, which is much smaller than 62% decay of NiO NTAs and those of other electrodes.[37-39]

Galvanostatic charge-discharge curves of Ni@NiO CSNPTAs in a half-cell at various current densities are shown in Figure 4d, which shows the symmetric nature in all charging/discharging curves, indicating good supercapacitive characteristic and superior reversible redox reactions. Figure 4e shows the summary plot of C_{sp} *vs* current density, which also indicates Ni@NiO CSNPTAs exhibit significantly enhanced supercapacitive performance compared with NiO NTAs. With charging/discharging rate increasing from 1.0 to 25.0 A/g, the Ni@NiO CSNPTAs show ~19% C_{sp} loss, which is much smaller than ~48% C_{sp} loss of the NiO NTAs. So this result also demonstrates Ni@NiO CSNPTAs have a much better rate capability than NiO NTAs. The Ni@NiO CSNPTAs also show good long-term cycle stability. After 1000 cycles, the C_{sp} retention of Ni@NiO CSNPTAs at 5.0 A/g is ~92%, which is much higher than ~55% C_{sp} retention of NiO NTAs as shown in Figure 4f. In addition, the surface morphology and mixed phases of the Ni@NiO CSNPTAs are well kept as shown in Figure 5 after 1000 cycles.

Based on the above results, Ni@NiO CSNPTAs as electrodes show large C_{sp}, excellent rate capability, and excellent cycle stability, and this can be attributed to the following advantages of electrode structures: *i*) the Ni@NiO core-shell structures can provide fast electron transport and improved charge-collection capacity; *ii*) the nanotube array structures of Ni@NiO CSNPTAs not only can avoid nanoparticle agglomeration but also can provide short ion diffusion paths and enable fast, reversible faradic reactions; *iii*) the porous and hollow nanostructures of Ni@NiO CSNPTAs obviously enhance utilization rate of electrode and also can provide large surface area for faradic reactions.

The capacitive performance of Ni@NiO CSNPTAs is further evaluated in a full cell set-up, and the asymmetric supercapacitors (ASCs) were assembled using Ni@NiO CSNPTAs as positive electrode and 3D-activated carbon (AC) as negative electrode (namely, Ni@NiO CSNPTAs//3D-AC ASCs). The electrochemical properties of 3D-AC electrodes are shown in Figure 6. To determine the operating voltage of ASC device, CVs of Ni@NiO CSNPTAs (red curve) and 3D-AC electrodes (black curve) were together

measured in solution of 1.0 M KOH at 100 mV/s, respectively, as shown in Figure 7a, which shows the voltage windows of Ni@NiO CSNPTAs and 3D-AC electrodes were well complementarity. Therefore, Ni@NiO CSNPTAs as positive electrode and 3D-AC electrodes as positive electrode are good candidates for ASCs. CVs of the Ni@NiO CSNPTAs//3D-AC ASCs at different cell voltages are shown in Figure 7b, and the maximum operating voltage is determined as 1.5 V, which is much wider than those of the conventional AC-based SCs (~1.0 V) and NiO-based SCs (~0.8 V). The enhancement of cell voltage will be a critical factor to enhance energy and power densities of the Ni@NiO CSNPTAs//3D-AC ASCs.

Figure 7c shows CVs of Ni@NiO CSNPTAs//3D-AC ASCs in a full cell set-up at different scan rates in cell voltage of 0~1.5 V in 1.0 M KOH solution. The dependence of C_{sp} of Ni@NiO CSNPTAs//3D-AC ASCs on scan rate is shown in Figure 7d. The C_{sp} of ASCs achieves 427 Fg^{-1} at 5 mV s^{-1} for whole device, which is much higher than those of other ASCs at the same scan rate.[40-41] The ASCs also show excellent rate capability as shown in Figure 7d, which shows high C_{sp} retention of ~67% with scan rate increasing from 5 to 100 mV s^{-1}. Galvanostatic charge/discharge curves of the Ni@NiO CSNPTAs//3D-AC ASCs at various current densities in cell voltage of 0~1.5 V are shown in Figure 7e, which shows good electrochemical capacitance behavior and fast Faraday redox reaction. The C_{sp} of ASCs at 2.2 A g^{-1} is determined to be 263 F/g. In addition, the ASCs show high C_{sp} retention of 89.4% with current density increasing from 2.2 to 22.2 A g^{-1} as shown in Figure 7f.

The long-term cycle stability of Ni@NiO CSNPTAs//3D-AC ASCs was examined in a full cell set-up at 100 mV s^{-1} and it is shown in Figure 8a. The ASCs show a high C_{sp} retention of 93% after 1000 cycles, which reveals the Ni@NiO CSNPTAs//3D-AC ASCs have an excellent cyclic performance compared with other ASCs.[42-43] The Ni@NiO CSNPTAs//3D-AC ASCs also show high energy density that is an another important parameter for evaluating the performance of ASCs. Ragone plot of the Ni@NiO CSNPTAs//3D-AC ASCs is shown in Figure 8b. The highest energy density can achieve 84.8 Wh kg^{-1}, which is much larger than other NiO or Ni(OH)-based ASCs, such as porous NiO//carbon ASCs,[44] NiO-Ni foam//AC,[45] and $Ni(OH)_2$/graphene//graphene,[46] as shown in Figure 8b. The Ni@NiO CSNPTAs//3D-AC ASCs also show much higher energy density than other ASCs, such as carbon nanotube/graphene//Mn_3O_4 nanopartic-

les/graphene ASCs (22.9 Wh/kg),[41] MnO_2 nanowire-SWNT//In_2O_3 nanowire-SWNT ASCs (25.5 Wh/kg),[47] and AC//MnO_2 nanorods ASCs (28.4 Wh/kg).[48] To show the feasibility of energy storage application, two Ni@NiO CSNPTAs//3D-AC ASCs were assembled in series for a demo as shown in inset in Figure 8a. Here we found that this ASC device could power a red light-emitting diode (LED) well for ~20 min after charging at 2.67 mA cm^{-2} for 40 s.

3. Conclusions

In summary, here the novel Ni@NiO CSNPTAs have been designed and fabricated via template-assisted electrodeposition that is a facile and high efficient method. The unique hollow structure, array structure, and metal/metal oxide core-shell nanostructures in the Ni@NiO CSNPTAs allow high efficient utilization of electrode with facilitated transports of ions and electrons. The fabricated Ni@NiO CSNPTAs showed superior electrochemical properties, such as high C_{sp}, excellent rate capability, and excellent long-term cycle stability. We also assembled the ASCs using Ni@NiO CSNPTAs as positive electrodes and 3D-AC as negative electrodes (namely Ni@NiO CSNPTAs//3D-AC ASCs), and they showed outstanding performance such as high C_{sp}, excellent cycle stability and high energy density. Here the certified perfect inosculation of compositionally and geometrically favourable factors provides a novel design strategy to fabricate nanotube array electrodes for ASCs with high performance.

4. Experimental Section

Fabrication of Ni@NiO core-shell nanoparticle tube arrays (CSNPTAs): All reagents used in study were analytical grade, and they were used directly without any purification. Ni@NiO CSNPTAs were fabricated by following steps via a facile ZnO nanorod template-assisted electrodeposition method:

(1) ZnO nanorod arrays (NRAs) templates were electrodeposited on Ti sheets (1.0 cm×1.0 cm) in solution of 0.01 M $Zn(NO_3)_2$+0.05 M NH_4NO_3 with current density of 0.5 mA·cm^{-2} at 70 °C for 90 min. The Ti sheets as substrate were prepared complying the following steps before each experiment: firstly polished by SiC abrasive paper from 300 to 800 grits, then dipped in HCl solution (5%) for 10 min and rinsed with acetone in ultrasonic bath for 5 min, and finally washed by distilled water.

(2) ZnO@Ni core-shell NRAs were fabricated via the electrodeposition of Ni nanoparticles on the surface of ZnO NRAs at a current density of 0.25 mA cm^{-2} in solution of 0.01M $Ni(Ac)_2$+0.05 M NH_4Ac+0.5 M H_3BO_3 for 60 min.

(3) The synthesized ZnO@Ni core-shell NRAs were then immersed in 3% $NH_3 \cdot H_2O$ solution for 2 h to remove ZnO template, and accordingly the Ni nanoparticle nanotube arrays (NPTAs) were fabricated. The fabricated Ni NPTAs were washed with doubly deionized H_2O three times.

(4) Ni@NiO CSNPTAs were finally fabricated by the partial oxidation of Ni NPTAs in air at 350 °C for 60 min. The oxidation of the Ni NPTAs was studied by thermogravimetric (TG) analysis using a NETZSCH TG 209F1 equipment under an atmosphere of air with a flow rate of 100 mL min^{-1} at the temperature of 35~800 °C with a heating rate of 5 °C min^{-1}. These fabricated Ni@NiO CSNPTAs were directly utilized as electrodes for supercapacitors (SCs) because they grew on Ti sheets that were good current collectors.

***Fabrication of 3D-activated carbon (AC)*:** 3D-AC electrode was synthesized by the following step: 85 wt% AC, 5 wt% carboxymethylcellulose, and 10 wt% butadiene styrene rubber were mixed and then were pressed into 3D-Ni foam.

Characterizations: The microstructures and surface morphologies of as-prepared samples were characterized by X-ray diffraction (XRD, Bruker, D8 ADVANCE), field emission scanning electron microscopy (SEM, JSM-6330F) and transmission electron microscopy (TEM, FEI-G2-F30, 300kV). Chemical-state analysis of as-prepared samples was carried out by X-ray photoelectron spectroscopy (XPS) using an ESCALAB 250 X-ray photoelectron spectrometer. For XPS spectra, the binding energy was calibrated using the C1s photoelectron peak at 284.8 eV as the reference. The loading of Ni@NiO CSNPTAs was analyzed by inductively coupled plasma atomic emission spectroscopy (ICP, SPECTRO).

Electrochemical measurements: A CHI 760D electrochemical workstation was utilized for electrochemical measurements. The electrochemical peroperties of Ni@NiO CSNPTAs and 3D-AC electrodes were studied in solution of 1.0 M NaOH in a half-cell (three-electrode electrolytic cell). The Pt sheet was used as a counter electrode and the saturated calomel electrode (SCE) with a double salt bridge system was utilized as the reference electrode. The cyclic voltammometry and galvanostatic charge/discharge experiments of the Ni@NiO CSNPTAs were performed between -0.2 and 0.6 V vs SCE at scan rates of 5~100 mV/s. The potential range of AC electrode was from -1.0 to 0.0 V vs SCE. Before measurements, the working electrodes of the Ni@NiO CSNPTAs and AC electrodes were impregnated in electrolyte for 30 min to ensure them thoroughly wet. Electrochemical impedance spectroscopy (EIS) was also measured to study the conductivity of Ni@NiO CSNPTAs in 1.0 M NaOH solution. The EIS was measured by applying an alternating-current perturbation of 10 mV over the frequency range of 1 Hz and 10 kHz at an open-circuit potential of 0.32 V. To study the feasibility of energy storage applications, the asymmetric supercapacitors (ASCs) were assembled using Ni@NiO

CSNPTAs as positive electrode and 3D-AC as negative electrode, namely Ni@NiO CSNPTAs//3D-AC ASCs. The cyclic voltammograms (CVs) and galvanostatic charge-discharge curves of the Ni@NiO CSNPTAs//3D-AC ASCs were measured in a full-cell system (two-electrode system) to determine their electrochemical performance by CHI 760D electrochemical workstation.

ACKNOWLEDGEMENTS

This work was supported by NSFC (51173212), Natural Science Foundation of Guangdong Province (S2013020012833), Fundamental Research Fund for the Central Universities (13lgpy51), SRF for ROCS, SEM ([2012]1707), the Project of High Level Talents in Higher School of Guangdong Province, and Open-End Fund of Key Laboratory of Functional Inorganic Material Chemistry (Heilongjiang University), Ministry of Education.

REFERENCES

1 X. Li, G. Meng, Q. Xu, M. Kong, X. Zhu, Z. Chu and A.-P. Li, *Nano Lett.,* 2011, **11**, 1704.

2 X. Lu, G. Wang, T. Zhai, M. Yu, J. Gan, Y. Tong and Y. Li, *Nano Lett.,* 2012, **12**, 1690.

3 D. R. Cummins, H. B. Russell, J. B. Jasinski, M. Menon and M. K. Sunkara, *Nano Lett.,* 2013, **13**, 2423.

4 S. H. Ahn, D. J. Kim, W. S. Chi and J. H. Kim, *Adv. Mater.*, 2013, **25**, 4893.

5 Z. Gan, X. Wu, X. Zhu and J. Shen, *Angew. Chem. Int. Ed.*, 2013, **52**, 2055.

6 T. Chen, L. Qiu, H. G. Kia, Z. Yang and H. Peng, *Adv. Mater.*, 2012, **24**, 4623.

7 S. Wang, E. Iyyamperumal , A. Roy, Y. Xue, D. Yu and L. Dai, *Angew. Chem. Int. Ed.*, 2011, **50**, 11756.

8 L. Yadgarov, R. Rosentsveig, G. Leitus, A. Albu-Yaron, A. Moshkovich, V. Perfilyev, R. Vasic, A. Frenkel, A. N. Enyashin, G. Seifert, L. Rapoport and R. Tenne, *Angew. Chem. Int. Ed.*, 2012, **51**, 1148.

9 M.-H. Park, Y. Cho, K. Kim, J. Kim, M. Liu and J. Cho, *Angew. Chem. Int. Ed.*, 2011, **50**, 9647.

10 L. Liu and E. Pippel. *Angew. Chem. Int. Ed.*, 2011, **50**, 2729.

11 Y.-G. Huang, B. Mu, P. Schoenecker, C. Carson, J. R. Karra, Y. Cai and K. S. Walton, *Angew. Chem. Int. Ed.*, 2011, **50**, 436.

12 S. Zhuo, Y. Xu, W. Zhao, J. Zhang and B. Zhang, *Angew. Chem. Int. Ed.*, 2013, **52**, 8602.

13 W. Yang, L. Zhang, Y. Hu, Y. Zhong, H. B. Wu and X. W. Lou, *Angew. Chem. Int. Ed.*, 2012, **51**, 11501.

14 M. Ye, D. Zheng, M. Lv, C. Chen, C. Lin and Z. Lin, *Adv. Mater.*, 2013, **25**, 3039.

15 M. Ye, J. Gong, Y. Lai, C. Lin and Z. Lin, *J. Am. Chem. Soc.,* 2012, **134**, 15720.

16 G. Zhang, B. Y. Xia, C. Xiao, L. Yu, X. Wang, Y. Xie and X. W. Lou, *Angew. Chem. Int. Ed.*, 2013, **52**, 8643.

17 M. Lahav, T. Sehayek, A. Vaskevich and I. Rubinstein, *Angew. Chem. Int. Ed.*, 2003, **42**, 5576.

18 H.-H. Li, C.-H. Cui, S. Zhao, H.-B. Yao, M.-R. Gao, F.-J. Fan and S.-H. Yu, *Adv. Energy Mater.*, 2012, **2**, 1182.

19 C. H. Cui, H. H. Li, J. W. Yu, M. R. Gao and S. H. Yu, *Angew. Chem. Int. Ed.*, 2010, **49**, 9149.

20 C. H. Cui, J.W. Yu, H. H. Li, M. R. Gao, H.W. Liang and S. H. Yu, *ACS Nano*, 2011, **5**, 4211.

21 C. H. Cui, H. H. Li and S. H. Yu, *Chem. Commun.*, 2010, **46**, 940.

22 N. Kang, J. Park, J. Choi, J. Jin, J. Chun, I. G. Jung, J. Jeong, J.-G. Park, S. M. Lee, H. J. Kim and S. U. Son, *Angew. Chem. Int. Ed.*, 2012, **51**, 6626.

23 X. H. Xia, J. Tu, Y. Q. Zhang, X. L. Wang, C. D. Gu, X. B. Zhao, H. J. Fan, High-quality metal oxide core/shell nanowire arrays on conductive substrates for electrochemical energy storage, *ACS Nano*, 2012, **6**, 5531.

24 X. Xia, D. Chao, X. Qi, Q. Xiong, Y. Zhang, J. Tu, H. Zhang, and H. J. Fan, *Nano Lett.*, 2013, **13**, 4562-4568.

25 V. Mazumder, M. Chi, K. L. More and S. Sun, *Angew. Chem. Int. Ed.*, 2010, **49**, 9368.

26 A.-L. Wang, H. Xu, J.-X. Feng, L.-X. Ding, Y.-X. Tong and G.-R. Li, *J. Am. Chem. Soc.*, 2013, **135**, 10703.

26 H. Xu, L.-X. Ding, C. Liang, Y.-X. Tong and G.-R. Li, *NPG Asia Mater.*, 2013, **5**, e69.

27 J.-H. Kim, K. Zhu, Y. Yan, C. L. Perkins and A. J. Frank, *Nano Lett.*, 2010, **10**, 4099.

28. (a) A. K. Singh, D. Sarkar, G. Khan and K. Mandal, *J. Mater. Chem. A*, 2013, **1**, 12759; (b) M. Yu, W. Wang, C. Li, T. Zhai, X. Lu and Y. Tong, *NPG Asia Mater*, 2014, **6**, e129.

29 Q. Lu, M. W. Lattanzi, Y. Chen, X. Kou, W. Li, X. Fan, K. M. Unruh, J. G. Chen and J. Q. Xiao, *Angew. Chem. Int. Ed.*, 2011, **50**, 6847.

30 F. Yuan, Y. Ni, L. Zhang, S. Yuan and J. Wei, *J. Mater. Chem. A*, 2013, **1**, 8438.

31 M. Ye, J. Gong, Y. Lai, C. Lin and Z. Lin, *J. Am. Chem. Soc.*, 2012, **134**, 15720.

32 P. Yang, Y. Ding, Z. Lin, Z. Chen, Y. Li, P. Qiang, M. Ebrahimi, W. Mai, C. P. Wong, and Z. L. Wang, *Nano Lett.*, 2014, **14**, 731.

33 T.-Y. Wei, C.-H. Chen, H. Chien, S. Lu and C.-C. Hu, *Adv. Mater.*, 2010, **22**, 347.

34 C.-C. Hu, K.-H. Chang, M. Lin and Y.-T. Wu, *Nano Lett.*, 2006, **6**, 2690.

35 G. D. Moon, J. B. Joo and Y. Yin, *Nanoscale*, 2013, **5**, 11577.

36 J. Fu, C. Zhao, J. Zhang, Y. Peng and E. Xie, *ACS Appl. Mater. Interfaces*, 2013, **5**, 7410.

37 R. B. Rakhi, W. Chen, D. Cha and H. N. Alshareef, *Nano Lett.*, 2012, **12**, 2559.

38 G. Yu, L. Hu, M. Vosgueritchian, H. Wang, X. Xie, J. R. McDonough, X. Cui, Y. Cui and Z. Bao, *Nano Lett.*, 2011, **11**, 2905.

39 Z. Gui, H. Zhu, E. Gillette, X. Han, G. W. Rubloff, L. Hu and S. B. Lee, *ACS Nano*, 2013, **7**, 6037.

40 L. Niu, Z. Li, Y. Xu, J. Sun, W. Hong, X. Liu, J. Wang and S. Yang, *ACS Appl. Mater. Interfaces*, 2013, **5**, 8044.

41 H. Gao, F. Xiao, C. B. Ching and H. Duan, *ACS Appl. Mater. Interfaces*, 2012, **4**, 7020.

42 X. H. Lu, X. Huang, S. L. Xie, T. Zhai, C. S. Wang, P. Zhang, M. H. Yu, W. Li, C. L. Liang and Y. X. Tong, *J. Mater. Chem.*, 2012, **22**, 13357.

43 X. Wang, W. S. Liu, X. H. Lu and P. S. Lee, *J. Mater. Chem.*, 2012, **22**, 23114.

44 D-W. Wang, F. Li and H-M. Cheng, *J. Power Sources*, 2008, **185**, 1563.

45 H. Inoue, Y. Namba, E. Higuch, *J. Power Sources*, 2010, **195**, 6239.

46 J. Yan, Z. J. Fan, W. Sun, W. Sun, G. Ning, T. Wei, Q. Zhang, R. Zhang, L. Zhi and F. Wei, *Adv. Funct. Mater.*, 2012, **22**, 2632.

47 P.-C. Chen, G. Shen, Y. Shi, H. Chen and C. Zhou, *ACS Nano*, 2010, **4**, 4403.

48 Q. Qu, P. Zhang, B. Wang, Y. Chen, S. Tian, Y. Wu and R. Holze, *J. Phys. Chem. C*, 2009, **113**, 14020.

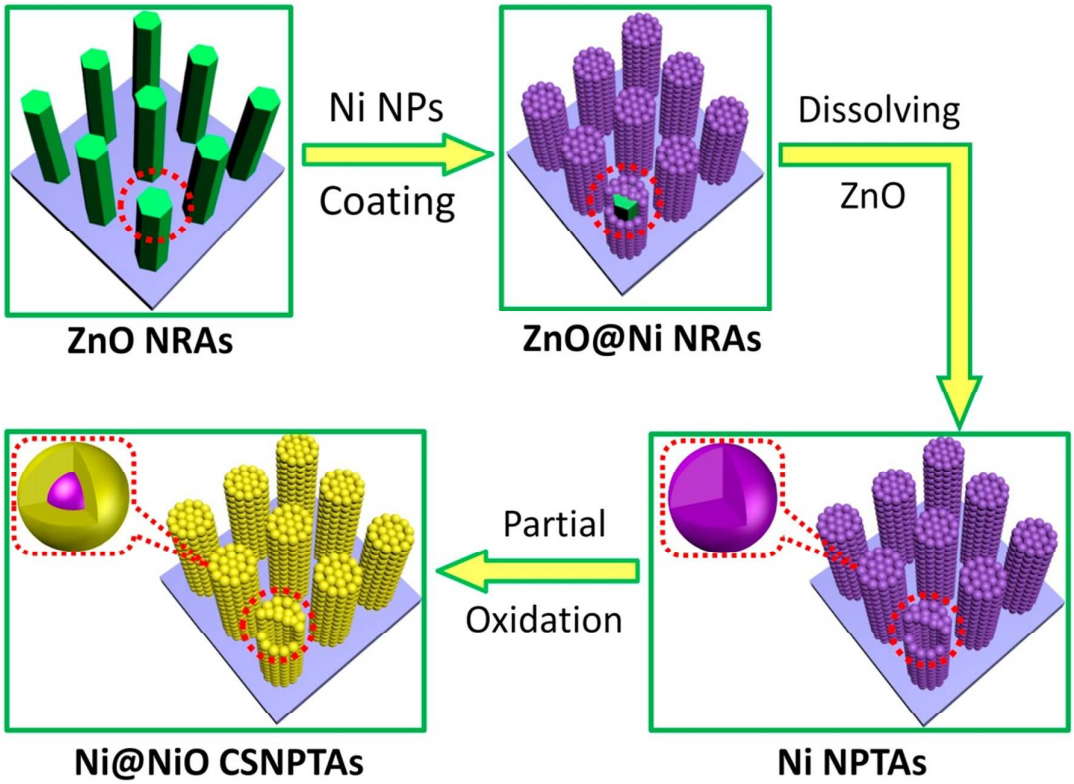

Scheme 1. Schematic illustration for the fabrication process of Ni@NiO CSNPTAs on the conductive substrate (NRAs: nanorod arrays; NPs: nanoparticles).

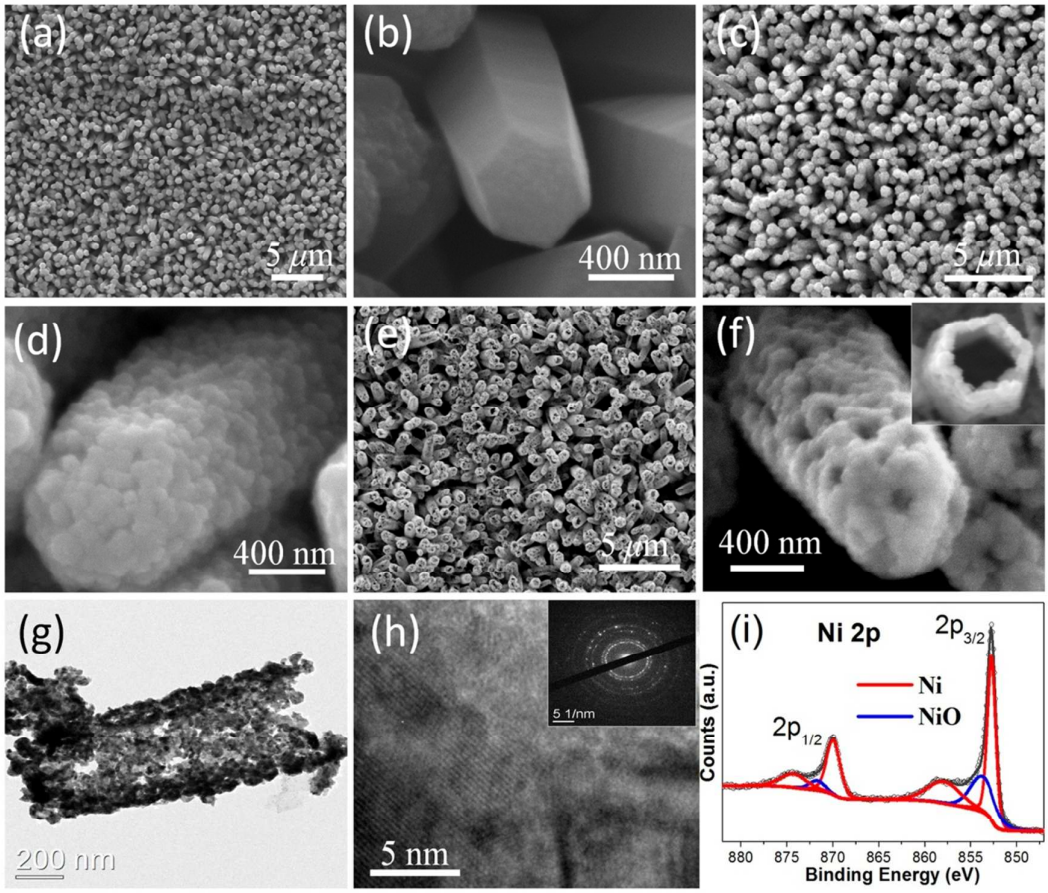

Figure 1. SEM images of (a-b) ZnO NRAs; (c-d) ZnO@Ni NRAs; and (e-f) Ni NPTAs; (g) TEM image, (h) HRTEM image and SAED pattern (inset) of a typical Ni nanotube; (i) XPS spectrum of Ni NPTAs.

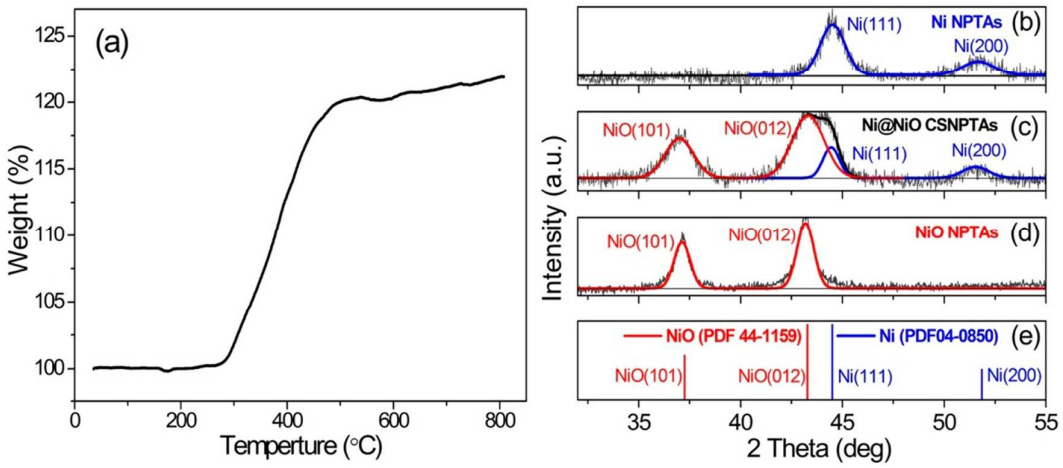

Figure 2. (a) TG curve of Ni NPTAs at a heating rate of 5 ^{0}C/min in air; (b) XRD pattern of Ni NPTAs before heat treatment; (c) XRD pattern of Ni NPTAs annealed in air at 350 °C for 60 min; (d) XRD pattern of Ni NPTAs annealed in air at 350 °C for 180 min; (e) The peaks correspond to the standardized peaks of NiO (PDF 44-1159) and Ni (PDF 04-0850).

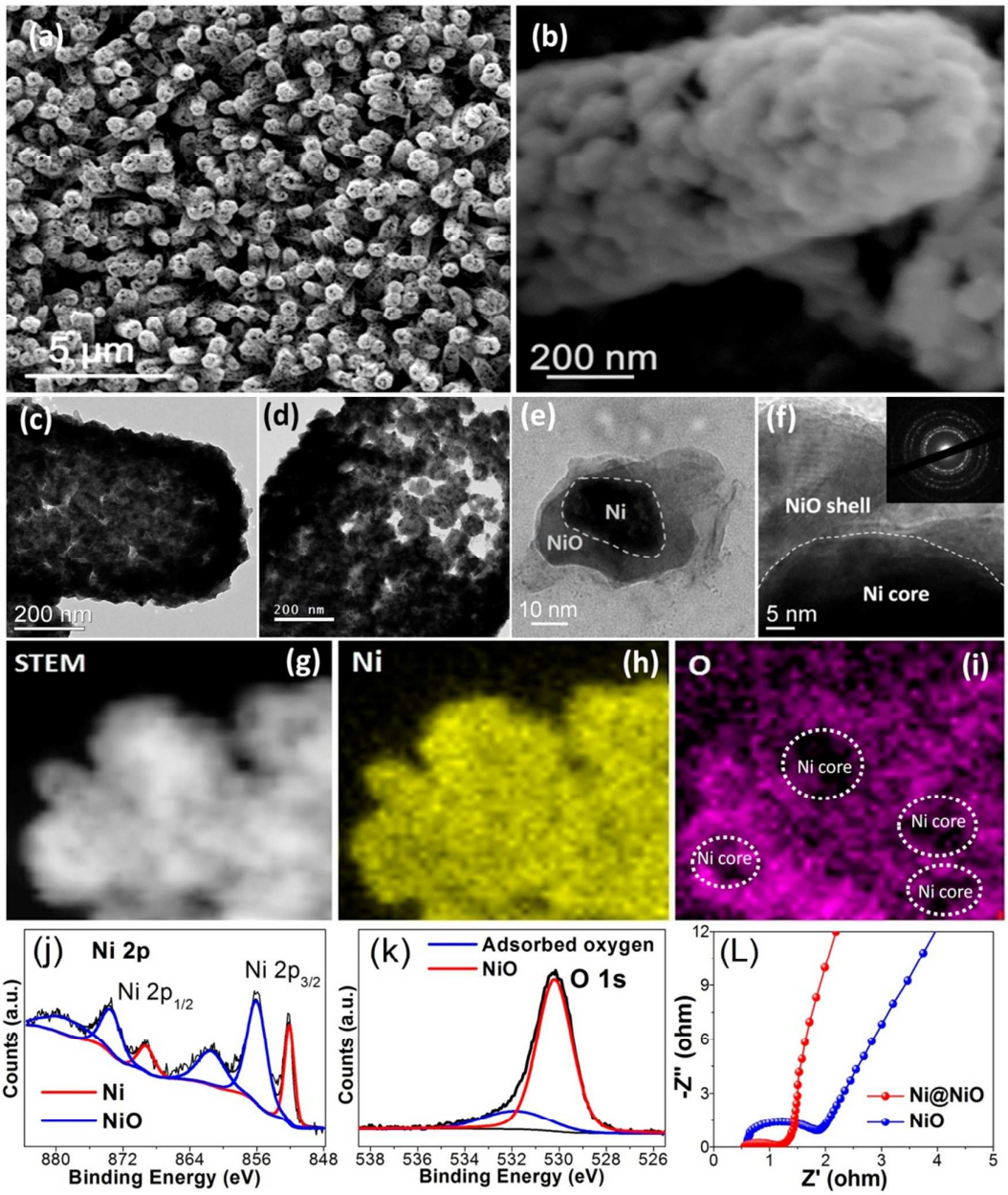

Figure 3. (a-b) SEM images of the Ni@NiO CSNPTAs; (c-d) TEM images of a typical Ni@NiO nanotube; (*e*) TEM image, (*f*) HRTEM image and SAED pattern (inset) of a typical core-shell nanoparticle in the Ni@NiO CSNPTAs; (*g*) STEM image of the core-shell nanoparticles in the Ni@NiO CSNPTAs and the corresponding EDS mappings of (*h*) Ni and (*i*) O; XPS spectra of (*j*) Ni_{2p} and (*k*) O_{1s} of the Ni@NiO CSNPTAs; (L) Nyquist plots of the Ni@NiO CSNPTAs and NiO NTAs.

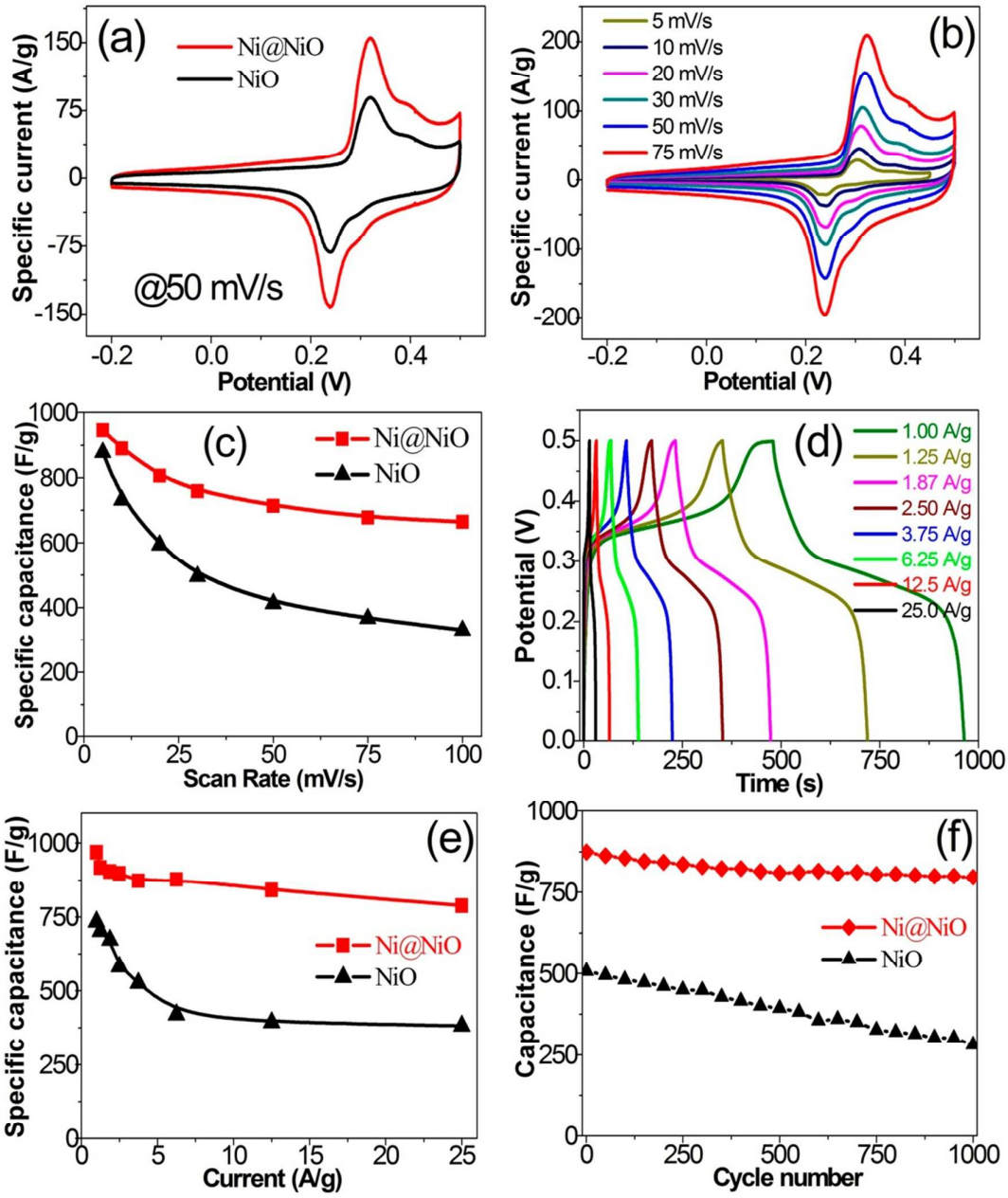

Figure 4. (a) CVs of the Ni@NiO CSNPTAs and NiO NTAs at 50 mV s^{-1} in a three-electrode system; (b) CVs of the Ni@NiO CSNPTAs at various scan rates; (c) C_{sp} of the Ni@NiO CSNPTAs and NiO NTAs as a function of scan rate; (d) Galvanostatic charge/discharge curves of the Ni@NiO CSNPTAs at various current densities; (e) C_{sp} of the Ni@NiO CSNPTAs and NiO NTAs as a function of current density; (f) Cycle life of the Ni@NiO CSNPTAs and NiO NTAs at current density of 5.0 A/g.

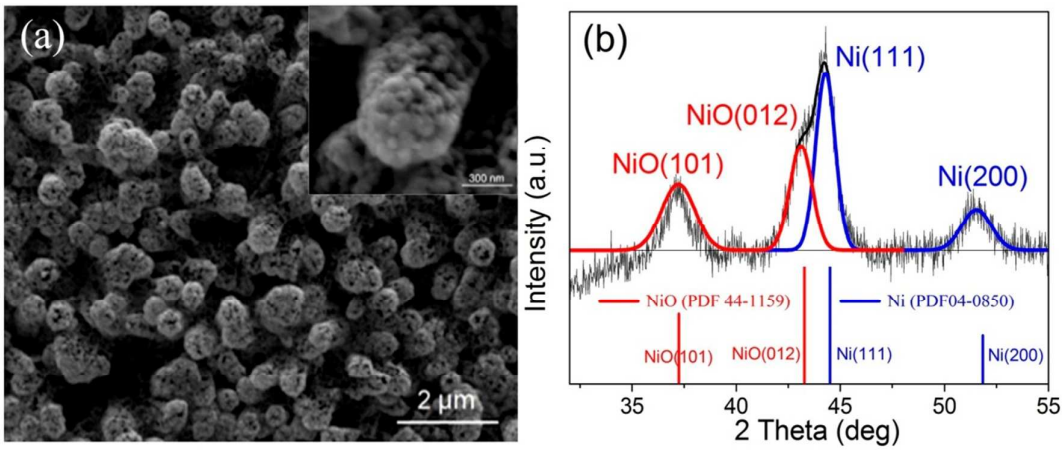

Figure 5. (a) SEM image and (b) XRD pattern of Ni@NiO CSNPTAs after 1000 cycles.

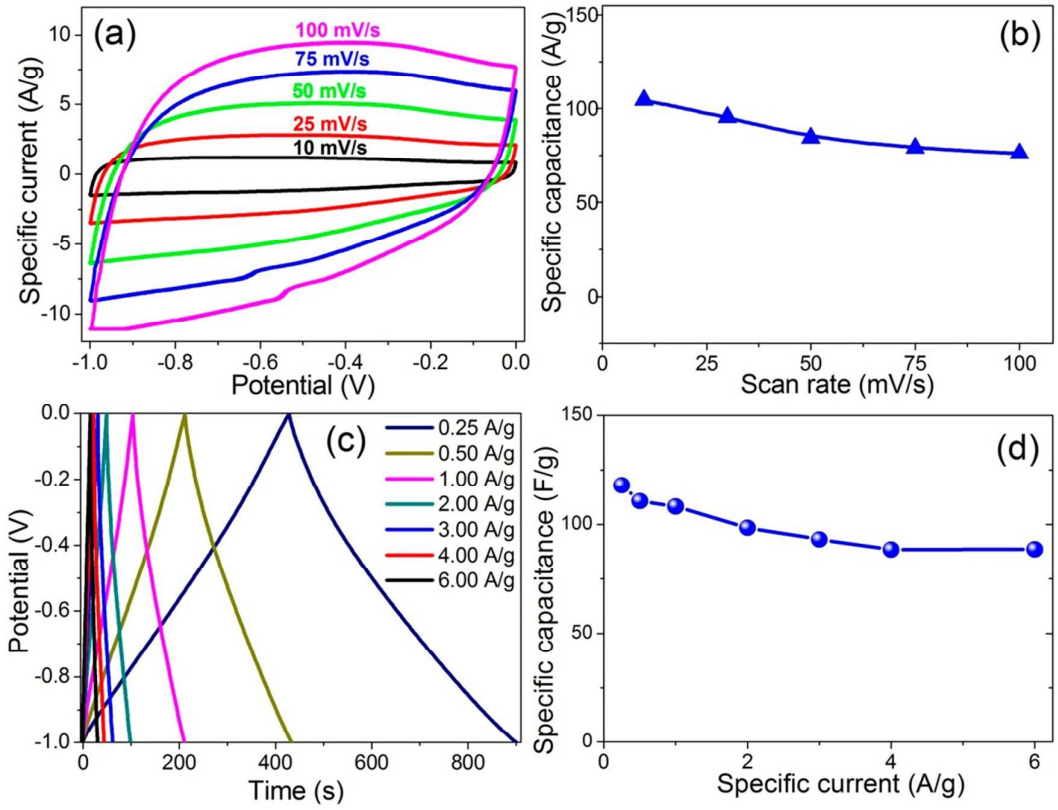

Figure 6. (a) CVs of 3D-AC electrodes at various scan rates; (b) C_{sp} of 3D-AC electrodes as a function of scan rate; (c) Galvanostatic charge/discharge curves of 3D-AC electrodes at various current densities; (d) C_{sp} of 3D-AC electrodes as a function of current density.

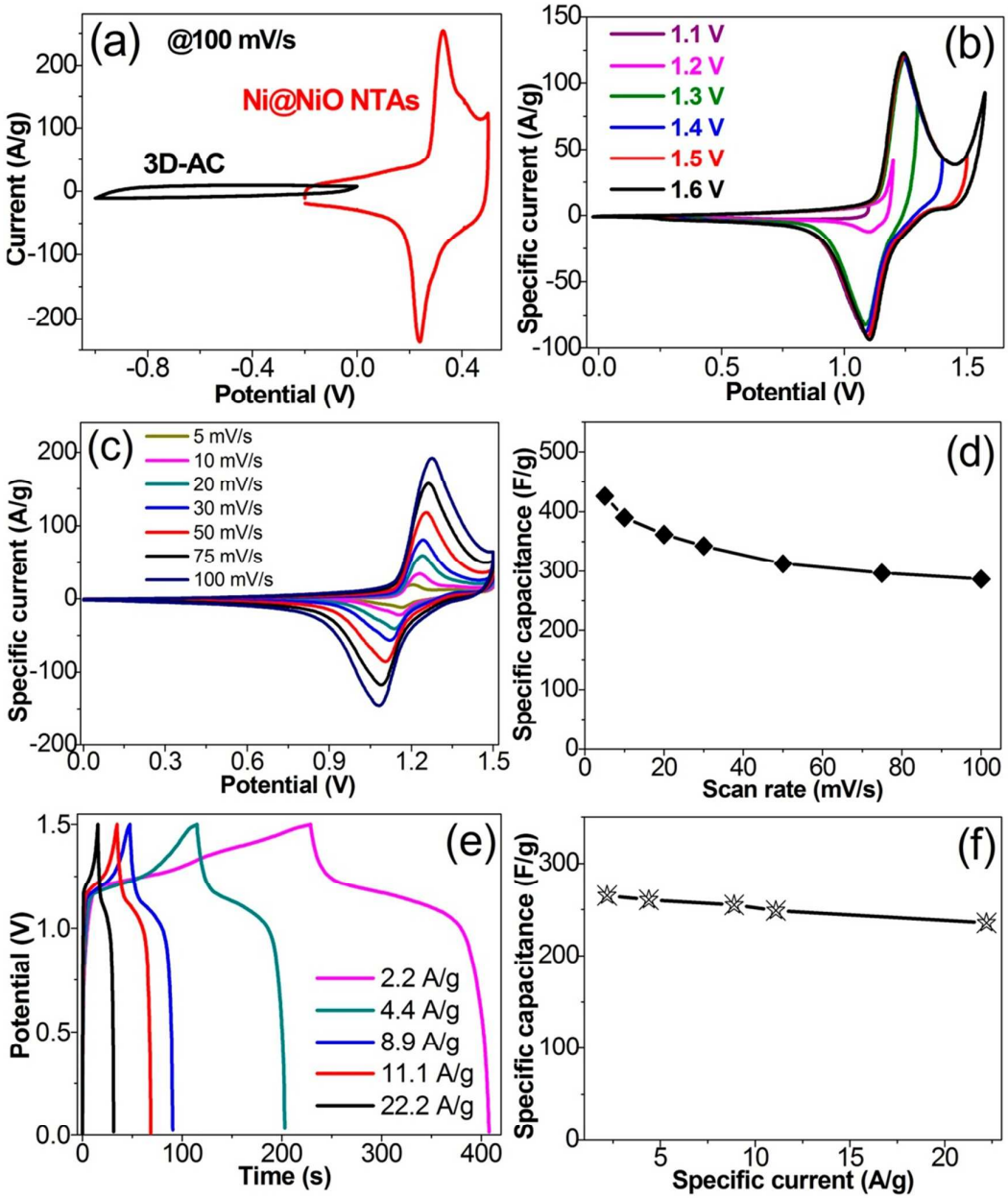

Figure 7. (a) CVs of the Ni@NiO CSNPTAs and 3D-AC electrodes at 100 mV s^{-1} in a two-electrode system; (b) CVs of the Ni@NiO CSNPTAs//3D-AC ASCs at different cell voltages; (c) CVs of the ASCs at various scan rates; (d) C_{sp} of the ASCs as a function of scan rate; (e) Galvanostatic charge/ discharge curves at different current densities for the ASCs operated within a potential window of 0~1.5 V; (f) C_{sp} of ASCs as a function of current density.

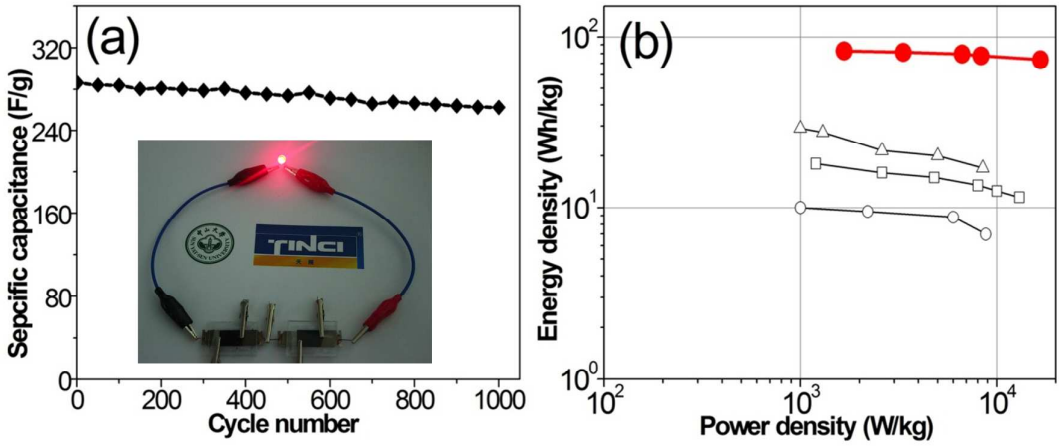

Figure 8. (a) Cycle life of the ASCs at a high scan rate of 100 mV s^{-1}; (b) Ragone plot related to energy and power densities of the Ni@NiO CSNPTAs//3D-AC ASCs (●) in comparison to NiO or $Ni(OH)_2$-based ASCs previously reported in literatures, namely porous NiO//carbon (○),[44] NiO-Ni foam//AC (□),[45] and $Ni(OH)_2$-graphene//graphene (Δ).[46] Inset shows a red LED (1.5 V) powered by a ASC device.

Graphical Abstract Picture